University of Cambridge
Department of Engineering
Trumpington Street
Cambridge, CB2 1PZ, UK

Drag Manipulation through Reversible Surface Dimpling and Ruffling

T C Hodges and K A Seffen

CUED/D-STRUCT/TR 226

Release date: September 2015

Preface

This work was originally conducted as a Part IIB MEng disseration project by Tom Hodges under the supervision of Keith Seffen from October 2013 to June 2014. Tom's final dissertation was awarded a distinction. This technical report follows from two unsuccessful attempts to publish key results from this dissertation in leading journals: The Journal of Fluid Mechanics and The Journal of Fluids and Structures. Our first paper was rejected outright because, as neophyte researchers in this subject area, we could not possibly make a worthwhile contribution; our second paper was received more warmly but rejected on firmer technical grounds. The reviewer made two comments relating to the design of our wind-tunnel specimens: that the aspect ratio of our cylinders was too small; and that circular end-plates fitted to them were also too small. Both give rise to "end-effects" which reduce the expected values of drag coefficient. Despite us arguing that these effects are the same for all results and thus only relative differences ought to matter, the reviewer noted that the character of the boundary later transition would be significantly affected, thereby invalidating our claim. We can live with this point but we stand by the work reported here, in particular, by the way in which surface ruffling (and not just dimpling) can result in successful drag manipulation—an effect that has received limited, if no, exposition in the academic literature. We are disappointed that none of the reviewers made *any* comment about this aspect of our work, either negative or positive: we therefore wonder about the inherent prejudices in the peer-review process; and the quality of that process.

Abstract

We consider a novel yet simple compliant surface, which greatly changes, and sometimes enhances, the aerodynamic properties of a smooth cylinder. The surface is a close-fitting foil sleeve, wrapped around the cylinder but not attached to it. The sleeve can also be axially compressed to yield a textured surface, analogous to the cylinder being dimpled. This process is reversible upon decompression, and the original smooth sleeve is recovered. We measured the drag of the compliant surfaces for Reynolds numbers in the range 1×10^5 to 6×10^5. When textured, the surface behaves as a roughened cylinder, precipitating boundary layer transition at a lower Reynolds number than for a smooth cylinder. When not textured, the sleeve moves dynamically on the cylinder in response to the flow. This ruffling initiates turbulence at lower speeds, which lowers drag as expected; but sometimes we do not see a short-lived drag crisis, rather a gradual diminution of the drag force. The extent of all of these effects is controlled by the initial gap-size between the sleeve and cylinder: within limits the tighter the fit, the closer the performance approaches that of the cylinder, and *vice versa*.

Keywords: compliant surface, sleeve, cylinder, dimples, reversible

1 Introduction

Normal flow around simple bluff bodies, such as spheres and cylinders, is fundamental in the study of aerodynamics, particularly for understanding the nature of drag forces and the boundary layer transition from laminar to turbulent flow. The onset of boundary layer turbulence is marked by the "drag crisis", which occurs at the critical Reynolds number: the drag crisis is a regime in which the drag coefficient, C_D, falls away over a short range of Reynolds numbers compared to the full range of practical flow speeds. The flow separates at a more rearwards point on the surface, leading to a smaller wake and a reduction in form drag; with increasing flow speed the separation points begin to migrate forwards, causing the drag to increase and "recover" asymptotically [1].

Surface roughening, artificial or natural, increases the propensity for boundary layer turbulence, which in turn diminishes flow separation and form drag. Compared to a smooth cylinder, a textured cylinder displays the drag crisis at a lower Reynolds number, leading to a lower drag at pre-critical Reynolds numbers and a higher drag at post-critical Reynolds numbers. The best known example of surface roughening for aerodynamic advantage is a golf ball, where roughening takes the form of a uniform pattern of manufactured indentations — "dimples" — of size approximately equal to 1% of the diameter. Roughening by gluing particulate grains, such as sand, all over a smooth surface is also possible, and was studied extensively for spheres in the early 1970s by Achenbach [2] and others. The size of dimples or grains measured relative to the body indicates the roughness scale (with typical "k/D" values between 0.5×10^{-2} and 1.5×10^{-2} in these studies). For the largest grain roughness, the critical Reynolds number can be lowered by as much as 80% compared to smooth [2], see Fig. 1(a), however, increasing the roughness diminishes the magnitude of

the reduction in C_D and exacerbates the level of drag in the turbulent regime, with C_D rising higher in the post-critical regime. Against comparable grain roughness, a dimpled golf ball experiences an even smaller drop in C_D but, atypically, does not show signs of drag recovery.

The drag coefficient of grain-roughened cylinders behave like their spherical counterparts but with C_D generally higher and with a proportionally smaller critical fall, see Fig. 1(b). Inspired by the uniform dimpling of golf balls, Bearman and Harvey [3] produced dimpled cylinders by machining rows of regularly spaced elliptical dimples all over a tube using a spherical cutter. During flow tests, they observed a performance similar to grain-roughened cylinders, with small differences in C_D in the laminar regime, depending on the position of the dimple line; but unlike the golf ball, post-critical values of C_D rose asymptotically once more. More recently, Choi *et al.* [4] conducted experiments on a dimpled sphere, which revealed a separation bubble forming within the dimples themselves: this triggers an unstable shear layer between the flow and the bubble, resulting in a large amount of local turbulence. This vorticity enables the flow to re-attach to the rear of the dimple with a "fuller" boundary layer profile, more resistant to separation. Other passive drag-reduction schemes have been devised, for example, by wrapping proud, helical strakes around the cylinder or by cutting lineal grooves into the surface. These grooves are typically of the same width and depth as a single machined dimple, and some drag benefits have been recorded for both span-wise and hoop-wise grooves provided they are precisely located [3]. Very recently, Butt *et al.* [5] studied cylindrical surfaces fully covered by machined hexagonal dimples, of similar topology to our textured cylinders; the dimples were either concave or convex, yielding reductions in drag coefficient by up to 35% compared to the smooth case.

Fixed dimpling or roughening is suitable when most of the flight envelope is in the Reynolds number range that benefits from having a lower drag, as per the golf ball. Active flow control is a method for modifying the aerodynamics in-situ, mainly of wings, for optimal matching of lift and drag forces throughout the duration of the flight. Because roughening mainly affects the properties of the drag crisis, controllable dimpling may shift the laminar-to-turbulent transition when the roughness of flight surfaces is altered, ideally in a short space of time and to varying degrees of roughness. The engineering challenge therefore lies in creating a surface with reversible, small-scale asperities, of comparable geometrical accuracy to those obtained from precision manufacturing. So-called smart materials such as electro-active polymers have been proposed, and implemented, in active dimple systems. However, instead of being static, they vibrate constantly in order to reduce skin friction rather than form drag [6]. This has been successfully demonstrated but its viability on full-scale structures remains unknown.

In this paper, we are concerned with reducing form drag using a smooth cylinder that can be reversibly "textured", see Fig. 2. A close-fitting membrane sleeve is wrapped around a solid cylindrical core giving way to an annular gap no larger than a few percent of the original diameter. The sleeve is longer than the core, so that it can be compressed axially between adjustable end-plates. It is also very thin and so buckles to create a uniform texture of surface dimples analogous to fixed roughening or dimpling, of comparable size

for drag reduction; by moving the end-plates apart, the original smooth surface is recovered. The system is mechanically very simple and offers remarkably high and repeatable uniformity both in terms of the layout of texture and the size of neighbouring cells. As shown by Seffen and Stott [7], the cell size is governed mainly by the size of the annular gap, with a larger gap giving a coarser texture and, hence, larger roughness, and *vice versa*. In a very recent paper, Terwagne *et al.* [8] develop another texturing mechanism utilising buckling for a sphere, which renders a dimpled surface akin to a golf ball. A surface membrane is attached to an elastic sphere, which can be evacuated and shrunk; the surface has to buckle bi-axially and periodically in order to comply with the core deformation. Reductions in drag force through dimpling are obtained and the experimental scheme can be switched between smooth and dimpled spheres in-situ. Presently, we cannot remotely actuate a texture although we are currently developing a scheme for motorising the end-plate movements. Instead, we have to set-up the sleeve differently outside of the wind tunnel before re-mounting it, but this does not subtract from our overall aims. Compared to the core by itself, we determine the drag coefficient profile for two cases, for Reynolds numbers, Re, in the range $1 \times 10^5 < \mathrm{Re} < 6 \times 10^5$.

The first case deals with textured sleeves, which behave as the familiar roughened cylinders. We show that the boundary layer transition from laminar to turbulent flow happens sooner, between 25% and 50% of the critical Reynolds number for the core alone, depending on the texture size compared to the smooth cylinder; during boundary layer transition, the fall-off in $\mathrm{C_D}$ is not as great, but afterwards it remains constant and does not rise within the post-critical regime as per the golf ball. Initially, we thought of doing no other tests, but we noticed that the sleeves can behave dynamically, especially at high flow speeds. This happens because each sleeve is thin and not rigidly attached to the core. Motivated by this sleeve deformation, we decided to remove texturing from consideration; in our second case, the sleeves are not compressed but only just held between the end plates on the core, and are initially smooth. Dynamic "ruffling" is a prominent feature of pre-critical flow, which reduces $\mathrm{C_D}$ compared to the core alone. In one of the two sleeves tested here, ruffling disappeared altogether after the drag crisis, with the sleeve becoming "locked" in shape; in the other, ruffling did not disappear, and the data shows no abrupt changes in $\mathrm{C_D}$ but rather a gradual tapering across the Reynolds numbers. Physically, this case is similar in prospect to so-called "compliant walls", inspired by the movement of supple skins in some aquatic mammals such as dolphins. As in skin, the wall is connected to a substrate through a layer of damping fluid, which permits enough flexibility for wall shape to adjust locally to the vagaries of the flow field. As detailed in [9], the crisis is *delayed* compared to smooth bodies, contrary to general dimpled bodies. In our sleeves, we observe an earlier crisis, in line with dimpling, but recall that there is no damping layer between the sleeve and the core. A closer example is loose-fitting sports clothing, as worn in, for example, ski-cross, in which a high drag force is reported across all Reynolds numbers, [10], again—quite different to our findings. The main aims of our paper are hence twofold: to introduce the benefits in drag reduction from a simply-made reversibly-textured surface; and to initiate study of drag on a close-fitting smooth surface, capable of limited, coupled movement with

the flow. In Section 2, we provide an overview of how to produce a textured cylinder and the experimental apparatus used for finding the drag coefficient. We present and discuss results in Section 3 before concluding in Section 4.

2 Experimental Set-up

(a) Manufacture of sleeve and texture formation

An uncompressed, smooth cylinder is shown in Fig. 2(a). It is made of Mylar, a polymer-backed aluminium foil used in the aerospace industry for its high toughness: it has a thickness of 44μm, Young's modulus of 1.01 GPa, and Poisson ratio of 0.38. It is mounted on (though not connected to) a stiff core between concentric end-plates, which act as platens for compression, see Fig. 2(b). Without the core, the sleeve would locally crumple during compression because it is a very thin-walled shell; the core stabilises this failure mechanism by inhibiting radial displacements over the precise annular gap formed initially between the core and the sleeve. Construction is shown in Fig. 2(c), where the core is used as a mandrel for wrapping the originally flat Mylar sheet, with a rod inserted between the two, before gluing along a narrow axial seam. Once the rod is removed, the annulus has a nominal radial width, $R_2 - R_1$, see Fig. 2(d). Local buckling spreads over the entire sleeve as compression proceeds, leading to a remarkably uniform diamond-shaped dimple pattern.

Seffen and Stott [7] describe the texture formation in detail, and note that the final geometry can be adequately described using simple "packaging" models, where the numbers of dimples around and along the cylinder, respectively, can be uncoupled. Circumferentially around the core, the dimple centre-lines can be approximated by a regular circumscribing polygon of length $2\pi R_2$, see Fig. 2(e). Denoting the "mis-match" in radii by an effective strain term, $\xi = R_2/R_1 - 1$, the dimple number, n, can be calculated:

$$\xi = \frac{\tan \pi/n}{\pi/n} - 1 \tag{1}$$

Figure 3 compares n above to measurements taken from Seffen and Stott [7] as well as the two sleeves from this study where $\xi = 0.25\%$ and 1%, respectively. Because of its simplicity Eqn 1 is an upper bound, but we see our sleeves fitting the experimental trend from elsewhere very well. Using the same polygonal geometry, we can approximate the dimple "height" as being the maximum radial displacement of a given vertex from the core, which we define as k in Fig. 2(e). As commonly used by others, one measure of surface roughness is the ratio of this height to the core diameter, D, equal to:

$$\frac{k}{D} = \frac{k}{2R_1} = \frac{1}{2}(\cos \pi/n - 1) \approx \frac{\pi^2}{4n^2} \quad \text{when } n \text{ is large} \tag{2}$$

This value ultimately depends on the mis-match, ξ, via n in Eqn 1, and using the two values in Fig. 3, we calculate $k/D = 8.5 \times 10^{-3}$ ($\xi = 0.25\%$) and $k/D = 2.04 \times 10^{-2}$ ($\xi = 1\%$), which closely match the dimpled roughness of Bearman and Harvey [3] and that of a typically golf ball ($\approx 9 \times 10^{-3}$).

The number of axial dimples is found to be governed by both the degree of compression and mis-match, and their interaction, and does not have a simple theoretical upper bound. Presently we shall simply note the numbers as counted for each mis-match employed here were 40 and 32, respectively. For completeness, we indicate schematically in Fig. 2(f) how compression is applied to the sleeve without impingement upon the core. First, the sleeve is made longer by a few percent so that it extends beyond the core ends; the end plates have a stepped profile that enables them to fit precisely inside the hollow core. The sleeve is slipped onto the core before inserting the collars, which are mounted concentrically on threaded studding using bolts; these are turned to realise axial movement between the collars up to the point where the step profile butts against the core ends—our textured state.

(b) Wind tunnel experiments

The cylinders were tested in the "Markham" wind tunnel in the Department of Engineering, University of Cambridge. It is a circulating tunnel used for research activities, with a working section of 1.1 m height and 1.7 m width, and observation windows for photographic recording during testing. The maximum flow speed is up to 60 m/s, giving a Reynolds number of $\mathrm{Re} = 6 \times 10^5$ for our specimens. The rig for mounting the Mylar sleeve normal to the flow inside the larger tunnel is presented in Fig. 4. The core and end-plates are supported by a pair of wires on either side connected directly to a force balance housed above the ceiling of the tunnel and out of flow; wires also drop vertically through the tunnel floor, where they are connected to a large mass in an oil bath for dampening translational vibration. Rotational vibration about the cylinder axis is dampened by means of a trailing frame, connected to another ceiling balance and oil-bath-mass via a central vertical wire. These wires are visible in the leading edge view in Fig. 4, where a textured sleeve has been installed. The total transverse length is limited to 600 mm by the wire locations, comprising a core length of 560 mm in addition to the widths of the adjustable end plates and wire attachment mechanism. A large diameter of cylinder is desirable, in order to increase the Reynolds number of flow, but this can increase the degree of flow blockage. Zdravkovich [11] suggests a nominal limit of 10% for the blockage ratio, beyond which the results must be corrected to account for transverse distortion of the flow: we chose a diameter of 154 mm, giving a blockage ratio of 4.9%.

After calibration, the force balance yields the drag force, D, on the rig at a given flow speed, V, which enables the drag coefficient to be calculated from $\mathrm{C_D} = D/(0.5\rho V^2 A)$. The drag force oscillates slightly in time around a mean value, and D is calculated to be an averaged value. The density of air, ρ, is found from the ideal gas law using the values of ambient temperature and pressure, and A is the frontal area, equal to the cross-sectional areas of the core/sleeve and end plates. The Reynolds number is given by Vd/ν, where

d is the cylinder diameter and ν is the kinematic viscosity. The drag coefficient of the rig by itself without the core was measured and found to be constant, with an average drag coefficient of 0.217 and standard deviation of 0.00534. This drag value was then subtracted from the absolute drag coefficient, to reveal the true coefficient, C_D, of the cylinder (and sleeve) alone. A detailed view of the suspension wires, end plates and wire attachment mechanism during calibration testing can be seen in Fig. 4.

Each of the textured sleeves ($\xi = 0.25\%$ and 1%) was made to be 574 mm long, giving an axial strain when fully compressed of 2.5% relative to the core length; for the uncompressed sleeve the core length is equal to 560 mm. All variations of drag coefficient with Reynolds number obtained are shown in Fig. 5.

3 Results and Discussion

The differences in C_D between the core cylinder, textured sleeves and smooth sleeve cases are remarkable. The core by itself behaves as a smooth cylinder, as expected, with a low Reynolds number, high drag force, laminar boundary-layer flow regime, followed by a high Reynolds number, low drag, turbulent boundary-layer regime. These regimes are separated by a well-defined drag crisis at $\mathrm{Re} \approx 4 \times 10^5$.

Our core cannot be treated, classically, as being "infinite" in the sense of exhibiting a uniform flow field along its length; entrainment of the wake around the cylinder ends occurs [12], which is known to reduce absolute values of C_D—in this case, by roughly 40% compared to the infinite cylinder. This does not invalidate the results presented as in this comparative study, the end effects were identical for every specimen tested; the variations in drag coefficient are a feature of the dimpled or non-dimpled sleeves and not a change in the magnitude of the end effects.

Compared to the core, both textured sleeves experience an immediate drag crisis at around $\mathrm{Re} = 1 \times 10^5$. This happens first for the 1% mis-match sleeve, where C_D reduces by roughly 50% compared to the smooth cylinder. The reduction in C_D for the 0.25% sleeve is more marked, being around 68%, at most, before recovering gradually, and more noticeably, than the 1% sleeve. Above $\mathrm{Re} = 4 \times 10^5$, however, both sleeves have C_D values above that for the core alone. Both textured C_D profiles behave as the machined and grain-roughened cylinders reported in [3], where surface roughness precipitates an earlier drag crisis, followed by low C_D values; drag recovery, however, is not entirely apparent for reasons discussed momentarily. Nonetheless, the difference between them is because the 1% sleeve is effectively rougher than the 0.25% sleeve according to Eqn 2. It is surmised that values of ξ smaller than 0.25% will result in C_D curves approaching that of the smooth cylinder.

Because the textured sleeves are compliant and not physically connected to the core, dimples were observed to distort under local flow conditions, and increasingly so for higher speeds where the aerodynamic forces were greater. Theory tells us that the flow pressure is positive on the front of the cylinder, before reducing as one moves around the circumference, resulting in a negative pressure on the upper and lower

surfaces; this has also been confirmed by experiments, for example, see [13, 14] and Fig. 8. For the 1% sleeve, the low pressure on the top and bottom surfaces caused a few of the dimples to reverse, or "pop out", at high Reynolds numbers, as shown in Fig. 6(a): a single dimple pops out, followed by others as the flow speed increases, occasionally with some of them merging to form a larger "blister". Dimples are able to resist this effect structurally up to a point, and this is complemented by the sleeve generally adhering to the core, as reported in [7]. The positive frontal pressure further impresses the sleeve upon the leading edge of the core, shown rather elegantly in Fig. 6(b). This causes the dimpled area in contact with the core to increase at expense of the interconnecting ridges narrowing. The number of dimples measured axially remains the same but the number circumferentially decreases due to the dimples lengthening around the cylinder as the flow speed increases, see Fig. 6(c). At the highest speeds, this lengthening is enhanced by the previous reversing of dimples, which creates more "space" into which the lengthening can expand. These two mechanisms are completely reversible; when the flow speed is dropped, the original uniform texture is recovered. The main parameter of this investigation, the initial dimple height, was fixed during each testing run; the "effective roughness" of the cylinder, however, is likely to have varied during testing due to the non-static dimple arrangement, as outlined above.

For the 0.25% dimpled case, the same deformation characteristics are observed, though they are seen at lower Reynolds numbers. At the highest speeds, however, popped dimples at the top and bottom of the sleeve begin to migrate circumferentially before coalescing into hoop-wise corrugations, see Fig. 7. These corrugations tend to bunch with little evidence of the original diamond pattern, and are connected by portions of smooth sleeve. This extensive deformation is also reversible, as shown, with the textured pattern being recovered when the flow speed is reduced. It is implied that 1% dimples have a greater inherent structural integrity than 0.25% dimples as the aerodynamic forces withstood before deformation are greater. Interestingly, informal tests on a 4% dimpled specimen resulted in large scale structural deformation at a very low Reynolds number, suggesting a "sweet spot" in terms of mis-match, where the structural properties of dimples are most favourable.

The performance of the uncompressed sleeves is different again. Returning to Fig. 5, the 0.25% sleeve behaves similarly to the core by tracking just below the latter's C_D curve. During laminar flow, the surface deforms dynamically by "ruffling" over its entire trailing half. On the leading side, the sleeve is pressed against the core, fitting exactly to the cylindrical surface. This creates an excess of sleeve material detached from the trailing surface of the core, which is more compliant in the sense of normal displacements than a textured sleeve. On the trailing edge, the flow has separated with a turbulent wake, and where the pressure locally varies, the detached sleeve is able deform spatially and dynamically. Such deformation has strong components chord-wise and circumferentially. This is a complex interaction which gives a sense of the coupling between the local variations of flow and deformation, however, some features can be observed: there is often a "ridge" of raised material on the uppermost and lowest surfaces; in addition, the excess

membrane on the rear of the cylinder can often, momentarily, be seen to take the shape of dimples formed as discussed earlier and in [7]. The seemingly random nature of the deformation period and magnitude echoes the unsteady turbulence of the cylinder wake. There is also some possible interaction with slight manufacturing imperfections in the seam of the sleeve, which is seated on the trailing edge of the cylinder in the centre of the wake (see Fig. 7(c)). After the crisis, this ruffling disappears almost instantaneously, resulting in the sleeve becoming "locked" in shape and giving the impression of being static.

Observations of the locked-in state suggest that the excess sleeve is concentrated in a gentle ridge on the uppermost and lowermost surfaces. Acknowledging that the pressure distribution for the sleeved cases was not measured, and may be altered from that reported in Fig. 8 by the presence of the sleeves themselves, we surmise that the altered sleeve behaviour is due to the changed pressure distribution on the surface of the cylinder following the drag crisis. Figure 8 shows that, following the drag crisis, the magnitude of the negative pressure on the upper and lower surfaces more than doubles, while at the rear of the cylinder the negative pressure drops very substantially. The pre-critical pressure distribution is of a roughly constant (negative) pressure on the rear of the cylinder, drawing the excess sleeve evenly around the rear of the cylinder, exposed to the turbulent wake. In contrast, the post-critical pressure distribution shows a definitive negative peak on the upper and lower surfaces. This pressure distribution supports the visual observation that in the post critical regime the excess sleeve is drawn to these upper and lower ridges, which are located forwards of the separation points and outside the turbulent wake - hence why no dynamic ruffling is observed.

For the 1% uncompressed sleeve, dynamic ruffling is more apparent because there is a greater arc-length of detached material on the trailing side. As the flow speed increases, ruffling persists without locking out; indeed, the ruffling becomes more "violent", with deformations moving at a higher frequency, presumably due to larger aerodynamic forces. Figure 5 does not display an obvious drag crisis for this case, rather an almost linear reduction in C_D with increasing Reynolds number. Although the exact mechanism remains unclear, it appears that there is some feedback with the membrane displacement increasing the level of turbulence in the boundary layer, hence, delaying separation points and reducing the drag: as the Reynolds number increases, the membrane disturbance becomes more violent, prompting greater levels of turbulence. The interaction between dynamic ruffling and drag is especially complex because the changing radial displacement of the membrane causes the shape of the bluff body to deviate slightly from the baseline case of a perfect cylinder. It is unclear why the 0.25 % and the 1 % non-dimpled cases behave differently.

For $\mathrm{Re} > 5 \times 10^5$, it is reasonable to assume that all specimens have turbulent boundary layers. Although the corresponding drag coefficients are smaller than for laminar boundary layer flow, there are wide variations in magnitude. The absence of a clear drag recovery throughout is also unusual. For ordinary bluff bodies, this is associated with the separation points moving forwards as the flow speed increases, thereby increasing the width of the wake. We believe that for our textured cylinders, dimples can inhibit this movement, after noting from the work on dimpled spheres in [4] that separation points remain fixed at a certain dimple

regardless of the post-critical Reynolds number. Recall for the 1% textured case that dimples remain in-situ during turbulence and can inhibit movement; in the 0.25% textured case, the surface was highly corrugated and, crucially, no longer dimpled—some drag recovery is evident in Fig. 5. The equivalent behaviour of uncompressed sleeves remains unclear, although we note that disregarding the deformation, and hence the drag recovery, of the 0.25% textured case, the minimum drag of the uncompressed sleeve corresponds strongly to the minimum drag of the textured cylinder for each mis-match. The 1% mis-match boundary layers have been tripped into turbulence to a greater extent than the 0.25% case, meaning that the 1% case boundary layer is less resistant to separation, leading to separation at an earlier point and to a larger wake and a higher post-critical drag.

4 Discussion and Conclusions

This study has shown that reversible dimples, made by compressing a tight-fitting sleeve on a cylinder, substantially and beneficially alter the flow characteristics of the cylinder in its pre-critical regime. The effective roughness afforded by the dimples is governed by the degree of initial radial mis-match between the sleeve and the cylinder, where a larger mis-match confers higher roughness and *vice versa*. Thus, it was found that a greater mis-match results in an earlier drag crisis but a larger turbulent drag coefficient: correspondingly, the larger mis-match showed less dimple distortion during turbulent flow, which we believe inhibits drag recovery because the surface maintains its dimpled shape and prevents flow separation points from moving forward. Uncompressed sleeves experienced dynamic ruffling on the trailing sides during laminar flow. For a larger mis-match, ruffling persists at higher speeds and the turbulent transition is gradual, whereas for a smaller mis-match, the ruffling dissipates quickly and the surface "rigidifies", with a crisis profile similar to that of a smooth cylinder.

Our research continues in developing actuation schemes for "switching" the texture on and off, so that at a given flow speed the drag coefficient changes by moving vertically between curves in Fig. 5, depending on the mis-match. These challenges are largely mechanical in conception, where we think of a scheme for powering the movement of end-plates in-situ. We are also considering material choices for the sleeve and the impact this has on ruffling, dimple distortions, and on the corresponding drag profile. However, there are still clear, open-ended aerodynamic questions and challenges remaining. We have presented results for two values of mis-match when comparing all surfaces; we have also informally tested a larger mis-match of 4%, which gave no improvement in performance because its compliance was too great. Our choice of mis-matches provides some guidance on the useful, or beneficial, range of mis-matches but it has, by no means, been investigated fully. We have only demonstrated matters for cylinders when other bluff and simple stream-lined bodies can be clear candidates for this type of technology. These all remain the focus of present study.

Acknowledgements

At CUED, we are grateful to Prof. Holger Babinksy for use of the Markham wind tunnel, and for technical support from Mssrs David Martin, Sam Flint and John Hazlewood. We thank Dr Will Graham and Ms Helen Webster for very helpful discussions. Research council funding did not support our work.

References

[1] J D Anderson Jr, *Fundamentals of Aerodynamics* (2007), McGraw-Hill International, pp. 279

[2] E Achenbach, The effects of surface roughness and tunnel blockage on flow past spheres, *Journal of Fluid Mechanics* (1974), 65(1), pp. 113-125

[3] P W Bearman and J K Harvey, Control of circular cylinder flow by use of dimples, *AIAA Journal* (1993), 31(10), pp. 1753-1756

[4] J Choi, W-P Jeon and H Choi, Mechanism of drag reduction by dimples on a sphere, *Physics of Fluids* (2006), 18(4) paper 041702

[5] U Butt, L Jehring and C Egbers, Mechanism of drag reduction for circular cylinders with patterned surface, *International Journal of Heat and Fluid Flow* (2014), 45, pp. 128-134

[6] S S Dearing, J F Morrison and L Iannucci, Electro-active polymer (EAP) "dimple" actuators for flow control: design and characterisation, *Sensors and Actuators A: Physical* (2010), 157, pp. 210-218

[7] K A Seffen and S V Stott, Surface texturing through cylinder buckling, *Journal of Applied Mechanics, ASME* (2014), 81(6), paper 061001

[8] D Terwagne, M Brojan and P M Reis, Smart morphable surfaces for aerodynamic drag control, *Advanced Materials* (2014) DOI: 10.1002/adma.201401403

[9] M Gad-el-Hak, Compliant coatings for drag reduction, *Progress in Aerospace Sciences* (2002), 38(1), pp. 77-99

[10] J J C Chua, F Konstantin Fuss and O Troynikov, Aerodynamics of loose sports garments, *Procedia Engineering* (2011), 13, pp. 370-375

[11] M M Zdravkovich, *Flow Around Circular Cylinders - Volume 2: Applications* (2003), Oxford University Press, pp. 827

[12] H Chanson, *Applied Hydrodynamics, An Introduction* (2013), CRC Press, pp. 96

[13] E Achenbach, Distribution of local pressure and skin friction around a circular cylinder in cross-flow up to Re = 5×10^5, *Journal of Fluid Mechanics* (1968), 34(4), pp. 625-639

[14] J P Batham, Pressure distributions on circular cylinders at critical Reynolds numbers, *Journal of Fluid Mechanics* (1973), 57(2), pp. 209-228

[15] J J Bertin and M L Smith, *Aerodynamics for Engineers*, fourth edition (2008), Prentice Hall, pp. 122

Figures

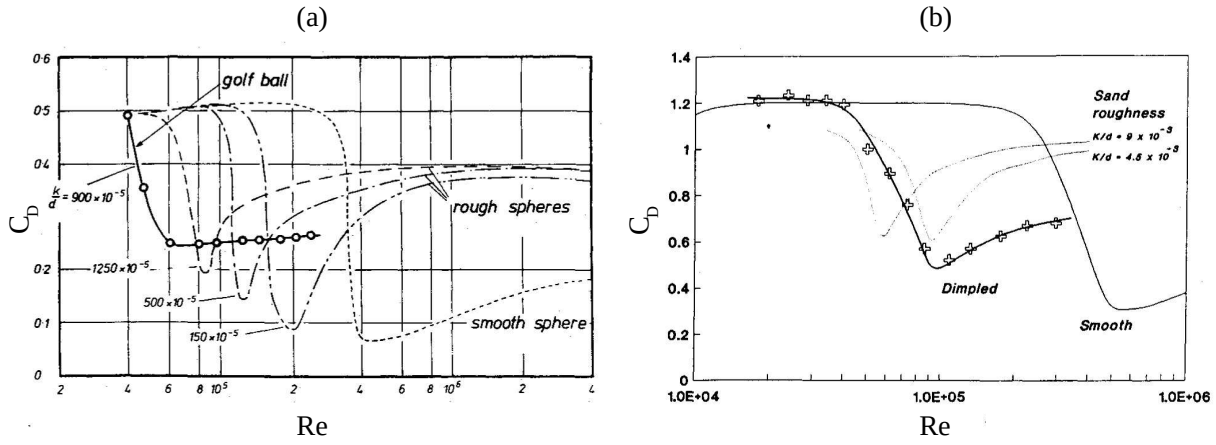

FIGURE 1: Drag coefficient, C_D, vs Reynolds number, Re, for (a) rough and smooth spheres, and (b) cylinders, both taken from [3]. Compared to the smooth cases in both, the boundary layer transition occurs at a lower Reynolds number for roughened bodies, and increasingly so for a higher surface roughness, as given by the size of k/D. The drag coefficient then recovers at a faster rate compared to the smooth case.

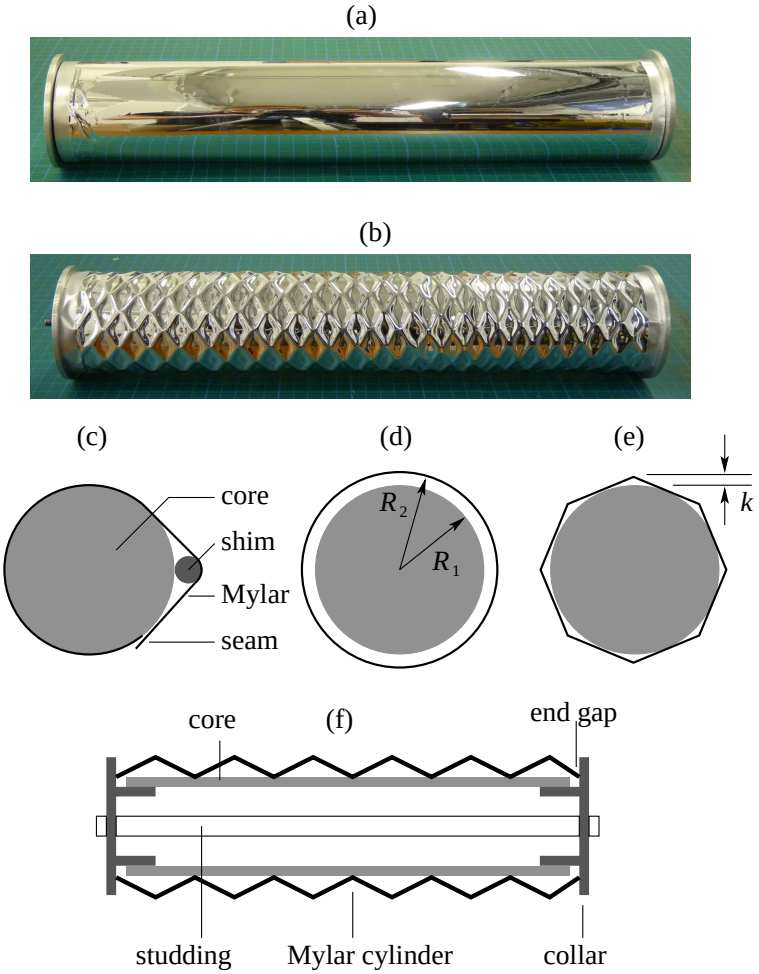

FIGURE 2: Operation of a textured cylinder. (a) Smooth cylindrical surface and (b) textured surface after axial compression, see (f). The surface is formed by wrapping a Mylar sleeve around a rigid core: inserting a rod creates a precision shim, (c), which enables an exact difference, (d), between the radius of the sleeve, R_2, and that of the core, R_1. This radial mis-match is essential for radial buckling of the sleeve and texture formation, as described in [7], where the number of dimples around the core was approximated by the number of sides of a circumscribing polygon, (e), of the same circumference as the sleeve: k is a surface roughness parameter equal to the vertex distance above the core. (f) Arrangement for enabling axial compression of the sleeve relative to the core. The end collars fit exactly inside the core radially but can slide axially due to the small end gap; their positions are adjusted and fixed by axial studding.

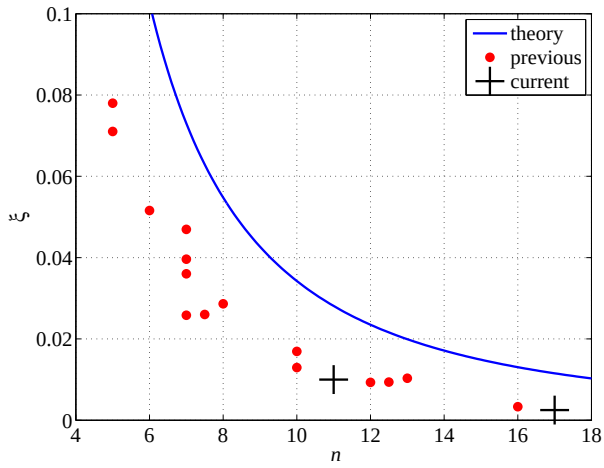

FIGURE 3: Number of circumferential dimples, n, for different radial mis-matches, ξ, between the inner core and textured sleeve, see Fig. 2. The "previous" results are taken from [7]; the current data are for $\xi = 0.25\%$ and 1%, where n is found by averaging the number of dimples at several axial positions; theory corresponds to Eqn 1.

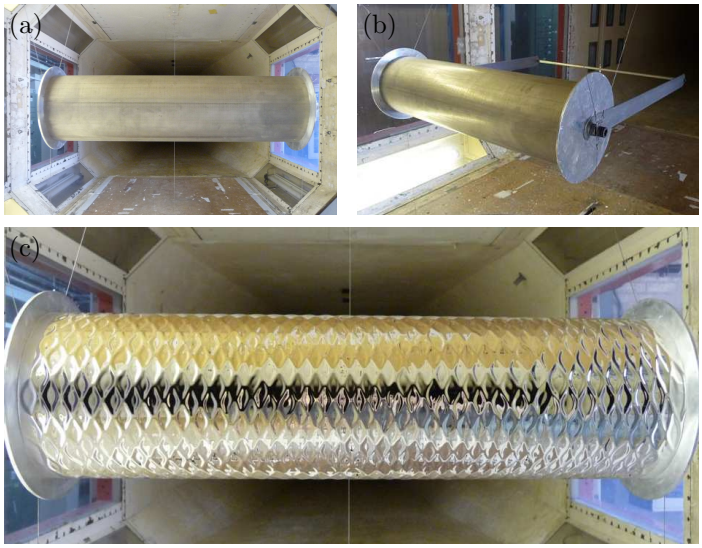

FIGURE 4: Larger wind tunnel testing rig. (a) Leading edge view of the cylindrical core with end plates: the cylinder length is 560 mm, and its diameter is 154 mm. (b) Perspective view to highlight the trailing arm for stabilising against pitching rotations. (c) Textured sleeve, $\xi = 0.25\%$, after compressing the ends relative to the core width by 2.5%. In all views, the wires are connected to the drag balance and dampening mechanism.

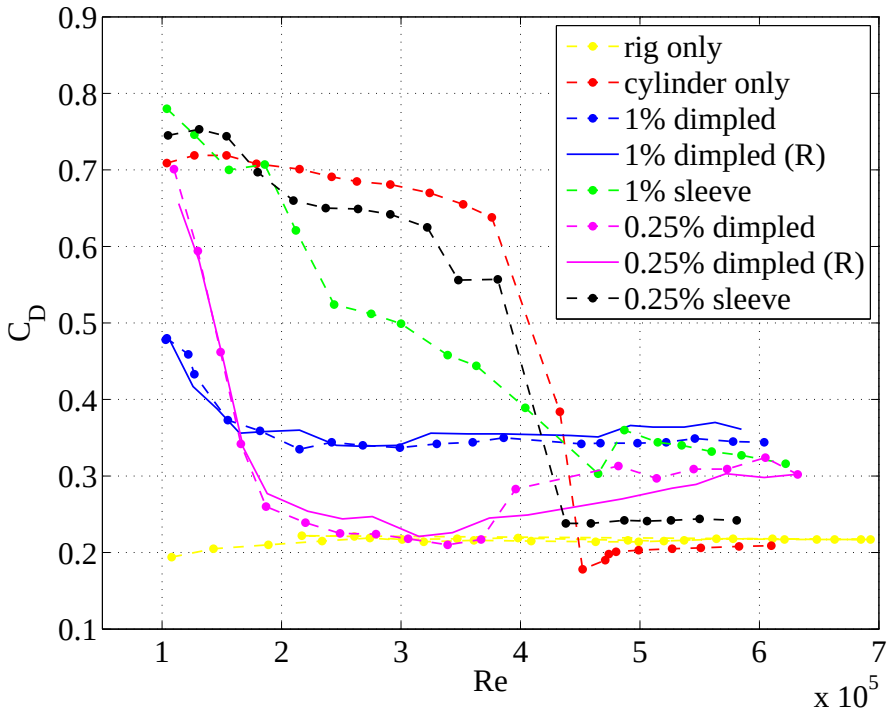

FIGURE 5: Drag coefficient, C_D, vs Reynolds number, Re, for cylinders and sleeves. In the legend, "dimpled" refers to textured sleeves; otherwise "sleeve" refers to an uncompressed smooth sleeve. (R) signifies a repeated experiment, and the mis-match strains, ξ, are 1% and 0.25%.

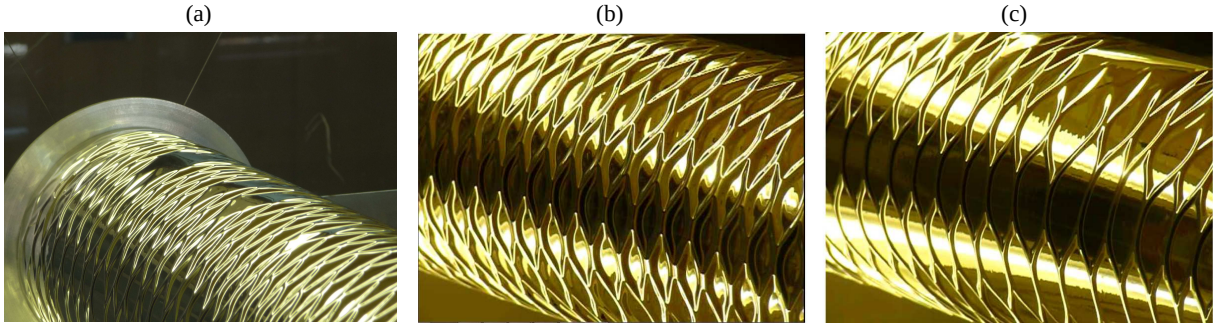

FIGURE 6: Distortion of the textured sleeve, $\xi = 1\%$, in the larger wind tunnel. (a) Some dimples on top have reversed direction and popped out under the local flow conditions. (b) The leading face of the sleeve is pushed onto the core, flattening the dimple contact areas; this is more pronounced in (c) at a higher flow speed, where the dimples now elongate circumferentially. Notice that the interconnecting ridges are narrower compared to (b) and that some of the reversed dimples on top have merged into a blister.

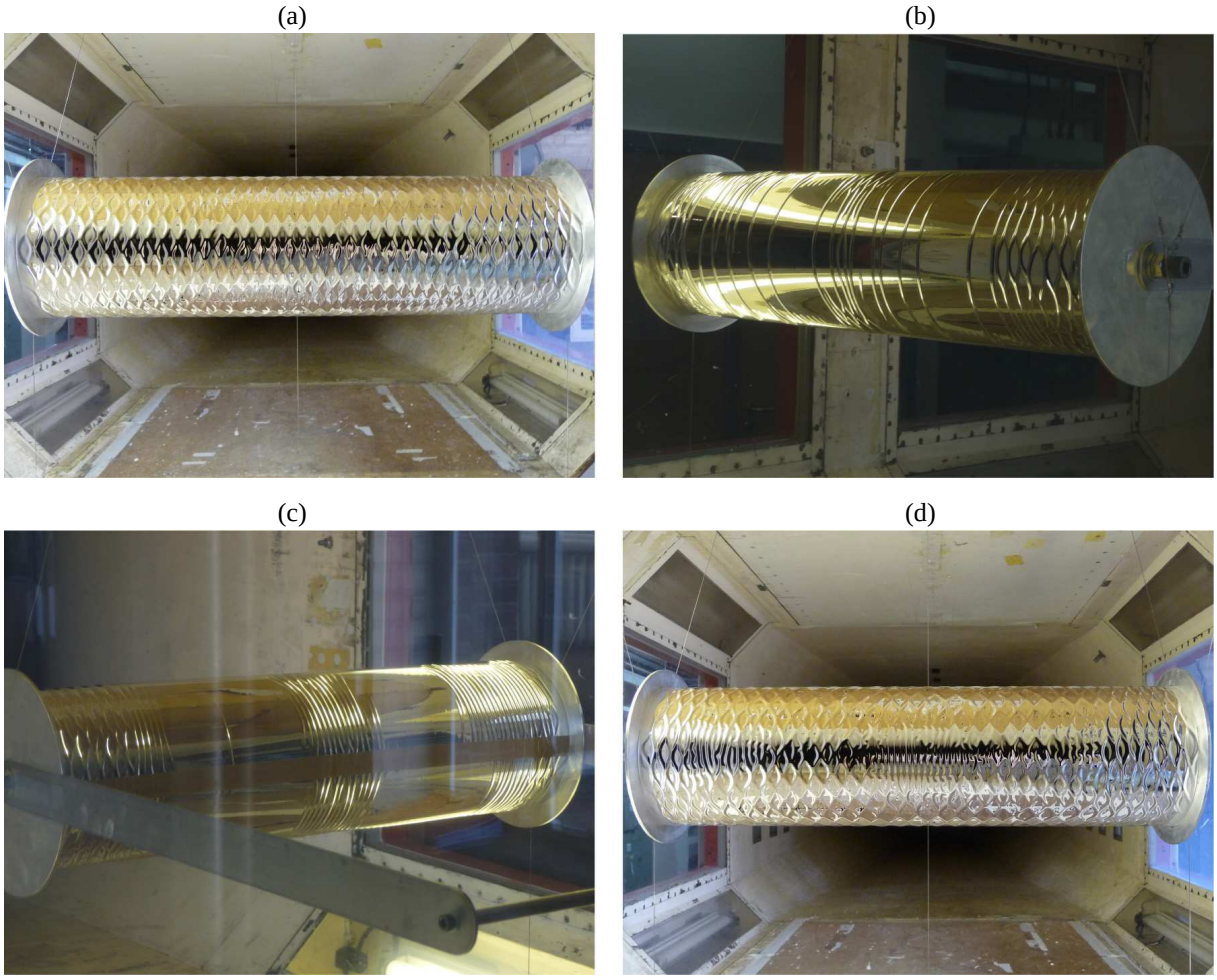

FIGURE 7: Distortion of the textured sleeve, $\xi = 0.25\%$, in the larger wind tunnel. (a) The initial set-up, as per Fig. 4(c). Formation of hoop-wise corrugations and smooth regions on the leading face, (b), and on the trailing face, (c), at high Reynolds numbers. The original texture from (a) is almost entirely recovered in (d), when the flow stops.

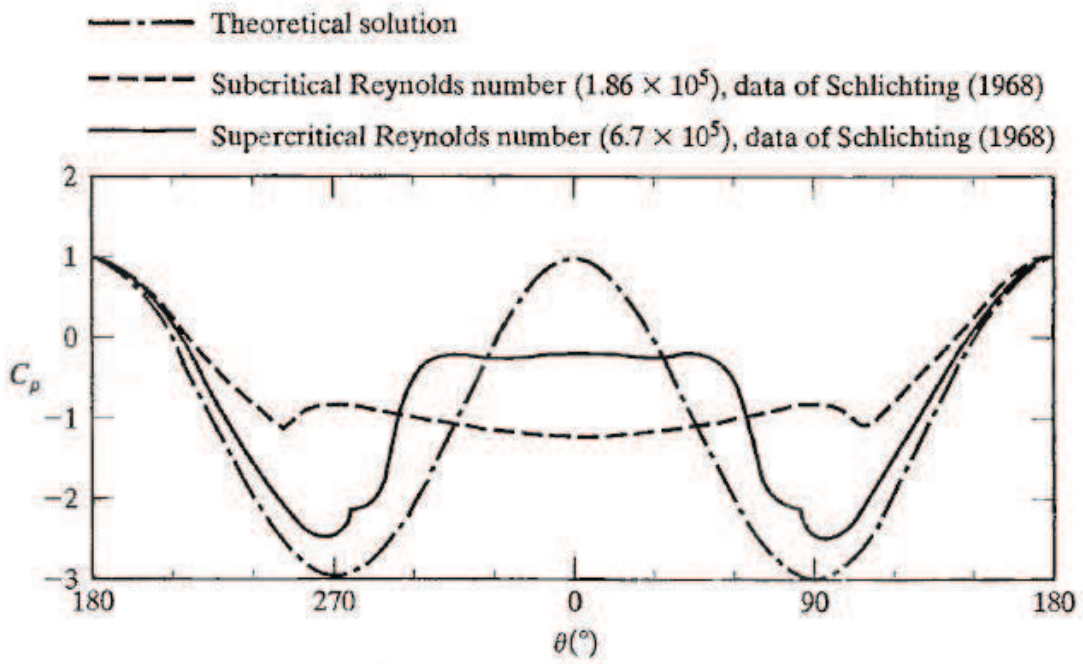

FIGURE 8: Pressure distribution due to flow around a cylinder, from Bertin and Smith [15]. Note that θ is measured from the rear most point on the cylinder; $\theta = 90^\circ$ therefore corresponds to the top (or bottom) and $\theta = 180^\circ$ to the front of cylinder.